

# Shape-space dynamics and geometric pattern formation in nonreciprocal slender bodies

Balázs Németh,<sup>\*</sup> Mohamed Warda,<sup>†</sup> and Ronojoy Adhikari<sup>‡</sup>  
*Department of Applied Mathematics and Theoretical Physics,  
 Centre for Mathematical Sciences, University of Cambridge,  
 Wilberforce Road, Cambridge CB3 0WA, United Kingdom*

Nonreciprocal interactions in active solids violate action–reaction symmetry and produce a net response to strain. Assuming invariance under Euclidean symmetries, we derive a shape-space formulation for the elastohydrodynamics of nonreciprocal slender bodies that separates intrinsic deformation from rigid motion. The resulting nonlinear reaction–advection–diffusion system represents a geometric flow whose activity-driven instabilities generate steady, oscillatory, and chaotic patterns. These manifest as rigid, swimming, and chaotic motion, linking nonreciprocal elastohydrodynamics to geometric pattern formation and unifying recent observations in slender active structures.

Slender elastic solids, spanning scales from eukaryotic flagella [1], hair [2], and spaghetti [3] to engineering structures [4], have long served as paradigmatic systems in mechanics. Following the geometric and nonlinear formulations of Euler, Kirchhoff, Timoshenko, and others [5–10], recent applications to plant growth [11], ciliary beating [12, 13], and locomotion [14, 15] require accounting for two features: immersion in a viscous fluid, where elastic and hydrodynamic forces compete in the overdamped elastohydrodynamic regime [16–19], and sustained conversion of chemical free energy into work [20], generating internal forces and torques that do not derive from an elastic potential.

Such systems may be viewed as active filaments [13, 21] or slender active solids [22, 23], with applications ranging from microscale transport [24, 25] to soft robotics [26, 27]. They have been realized experimentally using active colloids [28–30] and robotic platforms [31–34], and modeled theoretically as discrete bead–spring chains [35–37]. Within continuum theory, activity has primarily been introduced through nonclassical constitutive laws or boundary conditions [38]. In odd elasticity [39, 40], non-variational stress–strain relations produce non-Hermitian phenomena including unidirectional waves [32] and self-organized swimming [41]. Follower-force models employ nonconservative boundary loads that generate buckling and flapping instabilities [42–45]. In flagellar motility, activity is represented through effective force and torque densities acting on the elastic structure [46, 47].

Recent work has identified local sources of momentum [48] and angular momentum [49] in active solids as generic consequences of nonreciprocal interactions, which emerge upon coarse-graining microscopic degrees of freedom and violate action–reaction symmetry. When the microscopic interactions are invariant under Euclidean isometries, as in internally driven systems or hydrodynamically interacting systems far from boundaries, these sources depend only on strain [49]. Although the linear response of nonreciprocal solids is increasingly understood [22, 48, 49], the role of geometric nonlinearities,

which govern dynamics beyond linear instability thresholds, remains unexplored.

Here we study the elastohydrodynamics of a geometrically nonlinear slender solid driven by strain-dependent nonreciprocal force and torque densities. Exploiting invariance under rigid motions, we formulate the dynamics in shape space, decoupling intrinsic deformation from physical-space configuration [50]. The resulting dynamics is a geometric flow described by a reaction–advection–diffusion system for shape invariants [51]. We show that this system undergoes pattern-forming instabilities and bifurcations between fixed points, limit cycles, and chaos, which reconstruct in physical space as rigid motion, swimming, and chaotic dynamics. Nonreciprocal elastohydrodynamics thus becomes a problem of geometric pattern formation in shape space, enabling direct application of pattern-formation theory [52, 53] and providing a unified framework for recent observations in slender nonreciprocal active solids.

*Elastohydrodynamics.* We consider a slender elastic solid modeled as a thin uniform tube whose centerline is  $\mathbf{r}(u, t)$  and to whose cross-section is attached an orthonormal moving frame  $\mathbf{e}_1(u, t), \mathbf{e}_2(u, t), \mathbf{e}_3(u, t)$ , where  $u \in [0, L]$  is a Lagrangian parameter (not necessarily arclength) and  $t$  denotes time. Derivatives with respect to  $u$  and  $t$  are denoted by primes and dots, respectively. The kinematic equations are

$$\begin{aligned} \dot{\mathbf{r}} &= \mathbf{v}, & \dot{\mathbf{e}}_i &= \boldsymbol{\Omega} \times \mathbf{e}_i, \\ \mathbf{r}' &= \mathbf{h}, & \mathbf{e}'_i &= \boldsymbol{\Pi} \times \mathbf{e}_i, \end{aligned} \tag{1}$$

where  $\mathbf{v}, \boldsymbol{\Omega}$  are the translational and angular velocities and  $\mathbf{h}, \boldsymbol{\Pi}$  describe deformation. The index  $i = 1, 2, 3$  and the vector  $\mathbf{e}_1$  is normal to the cross-section.

Euclidean isometries act as  $\mathbf{r} \rightarrow \mathbf{R} \cdot \mathbf{r} + \mathbf{b}$ ,  $\mathbf{e}_i \rightarrow \mathbf{R} \cdot \mathbf{e}_i$  with  $\mathbf{R} \in \text{SO}(3)$ ,  $\mathbf{b} \in \mathbb{R}^3$ . Writing  $\underline{\mathbf{A}} = (A_1, A_2, A_3)$  for components  $A_i = \mathbf{e}_i \cdot \mathbf{A}$  in the moving frame, the six-dimensional variables  $E = (\underline{h}, \underline{\Pi})$  and  $V = (\underline{v}, \underline{\Omega})$  are isometry-invariant and describe the kinematics up to rigid motion. We refer to the set of  $E \in \mathbb{R}^6$  as the *space of shapes*. The configuration in physical space is recon-

structed by integrating the kinematics from  $E$  and initial data.

In the elasto-hydrodynamic limit, the overdamped balance laws are

$$\gamma^T \mathbf{v} = \mathbf{F}' + \mathbf{f}, \quad \gamma^R \boldsymbol{\Omega} = \mathbf{M}' + \mathbf{h} \times \mathbf{F} + \mathbf{m}, \quad (2)$$

with internal stresses  $\mathbf{F}, \mathbf{M}$  and force and torque densities  $\mathbf{f}, \mathbf{m}$ . This assumes that dissipative forces and torques are modeled by resistive force theory,  $\mathbf{f}^D = -\gamma^T \mathbf{v}$ ,  $\mathbf{m}^D = -\gamma^R \boldsymbol{\Omega}$ . More accurate nonlocal kernels from slender-body theory [54] should modify results quantitatively but not qualitatively. We assume the tube is free to move so that  $\mathbf{F} = \mathbf{M} = \mathbf{0}$  at its boundaries. Thus, overdamped motion is determined entirely by instantaneous balance of momentum and angular momentum.

*Shape-space dynamics.* Differentiating the kinematic equations and equating mixed partial derivatives gives the compatibility conditions

$$\dot{\mathbf{h}} = \mathbf{v}', \quad \dot{\boldsymbol{\Pi}} = \boldsymbol{\Omega}' + \boldsymbol{\Pi} \times \boldsymbol{\Omega}. \quad (3)$$

Eliminating the velocities between the balance laws and the compatibility conditions gives

$$\begin{aligned} \gamma^T \dot{\mathbf{h}} &= \mathbf{F}'' + \mathbf{f}', \\ \gamma^R \dot{\boldsymbol{\Pi}} &= \mathbf{M}'' + (\mathbf{h} \times \mathbf{F} + \mathbf{m})' + \boldsymbol{\Pi} \times (\mathbf{M}' + \mathbf{h} \times \mathbf{F} + \mathbf{m}). \end{aligned}$$

These equations close if the constitutive laws and boundary conditions only depend on the deformation. Projecting the above in the moving frame and using the identities  $\mathbf{e}_i \cdot \mathbf{A}' = (\underline{\mathbf{A}}' + \underline{\boldsymbol{\Pi}} \times \underline{\mathbf{A}})_i$  and  $\mathbf{e}_i \cdot \dot{\mathbf{A}} = (\underline{\dot{\mathbf{A}}} + \underline{\boldsymbol{\Omega}} \times \underline{\mathbf{A}})_i$ , we obtain

$$\dot{\underline{E}} = \mathcal{N}(\underline{E}), \quad \underline{E} = (h_1, h_2, h_3, \Pi_1, \Pi_2, \Pi_3), \quad (4)$$

where  $\mathcal{N}$  is a reaction–advection–diffusion (RAD) operator whose explicit form depends on the constitutive laws. This is a six-species pattern forming system in  $1 + 1$  dimensional spacetime and describes the geometric flow of the shape field  $E(u, t)$ . Diffusion arises from the elastic stresses while, crucially, geometric nonlinearities generate advection and reaction terms. The free boundary conditions depend only on  $E$  and the system closes in shape space.

*Mechanically linear media.* We now specify constitutive laws. Following [10], we take the harmonic elastic energy

$$\mathcal{E} = \frac{1}{2} \int_0^L du \left[ (\mathbf{h} - \mathbf{e}_1)^{\text{tr}} \mathbf{k}^T (\mathbf{h} - \mathbf{e}_1) + \boldsymbol{\Pi}^{\text{tr}} \mathbf{k}^R \boldsymbol{\Pi} \right], \quad (5)$$

which yields linear stress constitutive laws  $\mathbf{F} = \mathbf{k}^T \cdot (\mathbf{h} - \mathbf{e}_1)$ ,  $\mathbf{M} = \mathbf{k}^R \cdot \boldsymbol{\Pi}$ . We assume that the stiffness tensors simultaneously diagonalize in the moving frame so that  $\underline{\mathbf{k}}^T = \text{diag}(k_{\parallel}^T, k_{\perp}^T, k_{\perp}^T)$ ,  $\underline{\mathbf{k}}^R = \text{diag}(k_{\parallel}^R, k_{\perp}^R, k_{\perp}^R)$ .

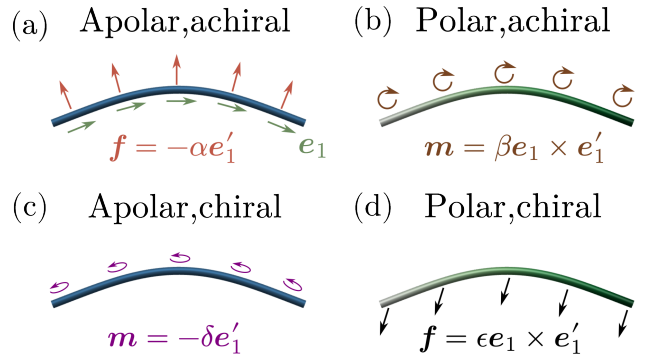


Figure 1. Active force and torque densities (6) and their symmetry classification [49]. (a) Normal force density proportional to curvature, similar to force densities in active nematics [55]. (b) Polar, achiral torque density proportional to curvature, leading to bend propagation [46]. (c) Apolar, chiral torque density, arising from, e.g., microscopic torque dipoles [56]. (d) Polar, chiral force density: an “odd” bending modulus generating transverse response to bending deformation.

Active contributions  $\mathbf{f}, \mathbf{m}$  arise from nonreciprocal interactions, e.g. coarse-grained hydrodynamic or chemical fields [19, 35]. The simplest strain-linear, transversely-isotropic form vanishing for straight configurations is [49]

$$\mathbf{f} = -\alpha \mathbf{e}'_1 + \epsilon \mathbf{e}_1 \times \mathbf{e}'_1, \quad \mathbf{m} = -\delta \mathbf{e}'_1 + \beta \mathbf{e}_1 \times \mathbf{e}'_1. \quad (6)$$

Here  $\beta, \epsilon$  break left–right symmetry, while  $\delta, \epsilon$  break mirror symmetry in the plane of the cross-sections. Although some terms are total derivatives, they are not equivalent to prestress due to boundary conditions. The RAD system corresponding to these constitutive choices is derived in the SM [57]. We now study its fixed points and bifurcations.

*Fixed points (stationary attractors).* In the absence of nonreciprocity, the homogeneous shape  $\underline{h} = \underline{e}_1, \underline{\Pi} = \underline{0}$ , corresponding to the straight configuration, is the unique fixed point of Eq. (4) and is linearly stable. Within the shape-space formulation, this state is a homogeneous stationary attractor. Upon reconstruction, such attractors correspond to rigid configurations with no intrinsic deformation or self-propulsion.

Nonreciprocal forcing alters this structure by generating curvature through the  $\alpha$  and  $\delta$  terms. As these coefficients are increased, the homogeneous attractor loses stability, giving rise to new inhomogeneous steady states in shape space, see Fig. 2. These emergent attractors correspond, upon reconstruction, to time-independent deformed configurations undergoing rigid motion in physical space.

To analyze the onset of instabilities, we linearize the shape equation about the homogeneous attractor. We nondimensionalize by rescaling lengths by  $L$  and times by the bending timescale  $T = \gamma^T L^4 / k_{\perp}^R$ . In the limit of large stretch, shear and twist moduli,  $k_{\perp}^R \ll k_{\parallel}^R, k_{\parallel}^T L^2, k_{\perp}^T L^2$

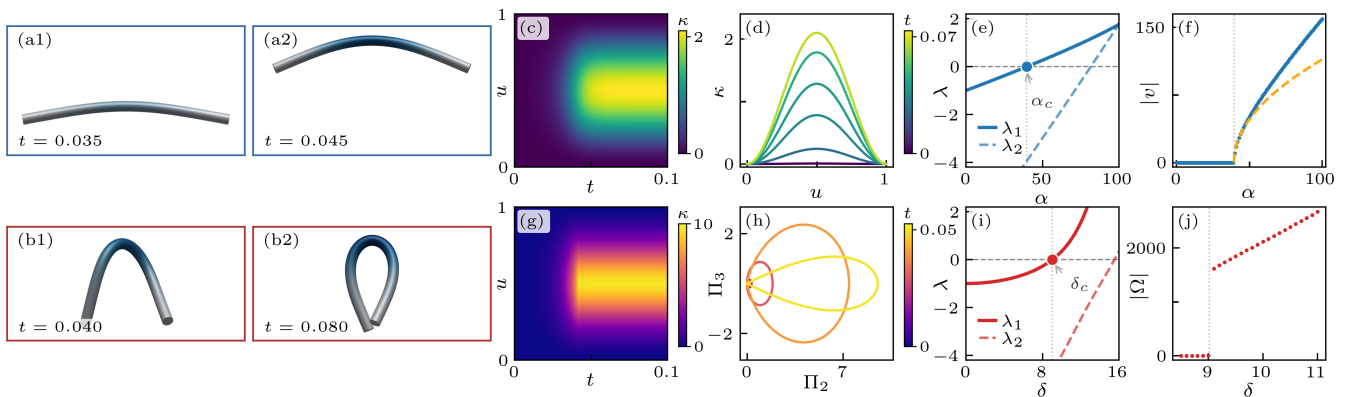


Figure 2. Fixed points of shape dynamics (see Movie 1 of the SM [57] for animations of the fixed point behavior). (a1)–(a2):  $\alpha = 50$ , self-propelling U-shape. The rod is shaded according to its scalar curvature. (b1)–(b2):  $\delta = 10$ , rotating hairpin shape. (c): Curvature kymograph of a rod with  $\alpha = 50$ . (d) Evolution of the curvature profile of the rod with  $\alpha = 50$ . (e) Leading eigenvalues of Eq. (7) as a function of  $\alpha$ , with other parameters zero. (f) Self-propulsion velocity from simulations as a function of  $\alpha$ . The dashed line is the prediction  $v \approx 14.7\sqrt{\alpha - 4\pi^2}$  from a weakly nonlinear analysis. (g) Curvature kymograph of a rod with  $\delta = 10$ . (h) Evolution of the shape of the rod with  $\delta = 10$ . (i) Leading eigenvalues of Eq. (7) as a function of  $\delta$ , with other parameters zero. (j) Angular velocity from simulations as a function of  $\delta$ .

and  $\gamma^R \ll \gamma^T L^2$ , the dynamics of  $\underline{h}$  and  $\Pi_1$  separate in time scale from the dynamics of  $\Pi_2$  and  $\Pi_3$ . This defines a slow manifold corresponding to the filament limit, in which the rod is inextensible ( $|\mathbf{r}'| = 1$ ) and unsharable ( $\mathbf{r}' \parallel \mathbf{e}_1$ ). In this regime, the dynamics is naturally expressed in terms of the complex curvature  $\Pi = \Pi_2 + i\Pi_3$ , which encodes both bending and torsion of the centerline.

On this slow manifold, stability is governed by the linear operator

$$\dot{\Pi} = -\Pi'''' - \mu\Pi''' - \nu\Pi'', \quad \Pi = \Pi_2 + i\Pi_3, \quad (7)$$

where  $\mu = (\beta + i\delta) \times L/k_{\perp}^R$  and  $\nu = (\alpha - i\epsilon) \times L^2/k_{\perp}^R$  are nondimensional complex-valued parameters encoding the strength of nonreciprocal forcing. The stability of the homogeneous attractor is determined by the spectrum of this operator with boundary conditions  $\Pi = \Pi' = 0$  at both endpoints, which predicts the onset of instabilities at critical values  $\alpha_c = 4\pi^2$  and  $\delta_c \approx 8.99$ , in excellent agreement with numerical simulations.

Beyond these thresholds, the stationary attractor loses stability and is replaced by new attractors in shape space. For  $\alpha > \alpha_c$ , a supercritical pitchfork bifurcation produces a branch of self-propelling U-shaped configurations, consistently with recent theoretical and experimental observations in active colloidal chains and chemically active filaments [21, 35, 37, 38, 58]. Weakly nonlinear analysis shows that the associated translational velocity scales as  $v \simeq 14.7\sqrt{\alpha - \alpha_c}$  near onset, see Fig. 2(f). Averaging the equations of motion over a planar shape self-propelling with speed  $v$ , we find the relation

$$v = 2\alpha \sin(\bar{\kappa}/2) \quad (8)$$

between the average scalar curvature  $\bar{\kappa} = \int_0^1 \kappa du$  of the

rod and its speed, yielding an exact nonlinear generalization of the result reported in [35].

For an apolar, chiral rod with  $\delta \neq 0, \alpha = \beta = \epsilon = 0$ , a distinct instability leads to rotating hairpin structures associated with global rigid rotation in physical space. With increasing  $\delta$ , we observe a helical buckling instability at a critical value  $\delta_c \approx 9$  [49, 59, 60], after which the rod settles into a rotating hairpin that undergoes global rigid rotation, with the amplitude jumping discontinuously at the bifurcation. In both cases, the new steady states remain fixed points in shape space but correspond to nontrivial rigid motion upon reconstruction.

The fixed points in shape space are robust to perturbations in the parameters but acquire qualitatively new features depending on the symmetry of the rod. At a fixed  $\alpha > \alpha_c, \delta = \epsilon = 0$ , breaking polar symmetry by a small  $\beta$  tilts the stationary U-shape, leading to a net torque on the rod and planar global rotating motion, while a small  $\epsilon$  at  $\alpha > \alpha_c, \beta = \delta = 0$  adds transverse forces, giving rise to chiral out-of-plane rotating motion. Higher modes also become unstable when  $\alpha$  is increased further, and we find rotating stationary shapes even in the absence of polar or chiral terms [57].

*Limit cycles (periodic attractors).* Beyond stationary attractors, RAD systems generically support oscillatory attractors arising through Hopf bifurcations. Exploring the nonreciprocal parameter space, we identify a regime in which the shape dynamics of a polar, achiral rod ( $\alpha, \beta \neq 0, \delta = \epsilon = 0$ ) evolves onto a stable limit cycle, see Fig. 3.

As  $\alpha$  is increased at fixed  $\beta \gtrsim 5$ , a pair of complex-conjugate eigenvalues of the linearized dynamics crosses the imaginary axis, see Fig. 3(d), and the stationary attractor loses stability. The system is thereby replaced by

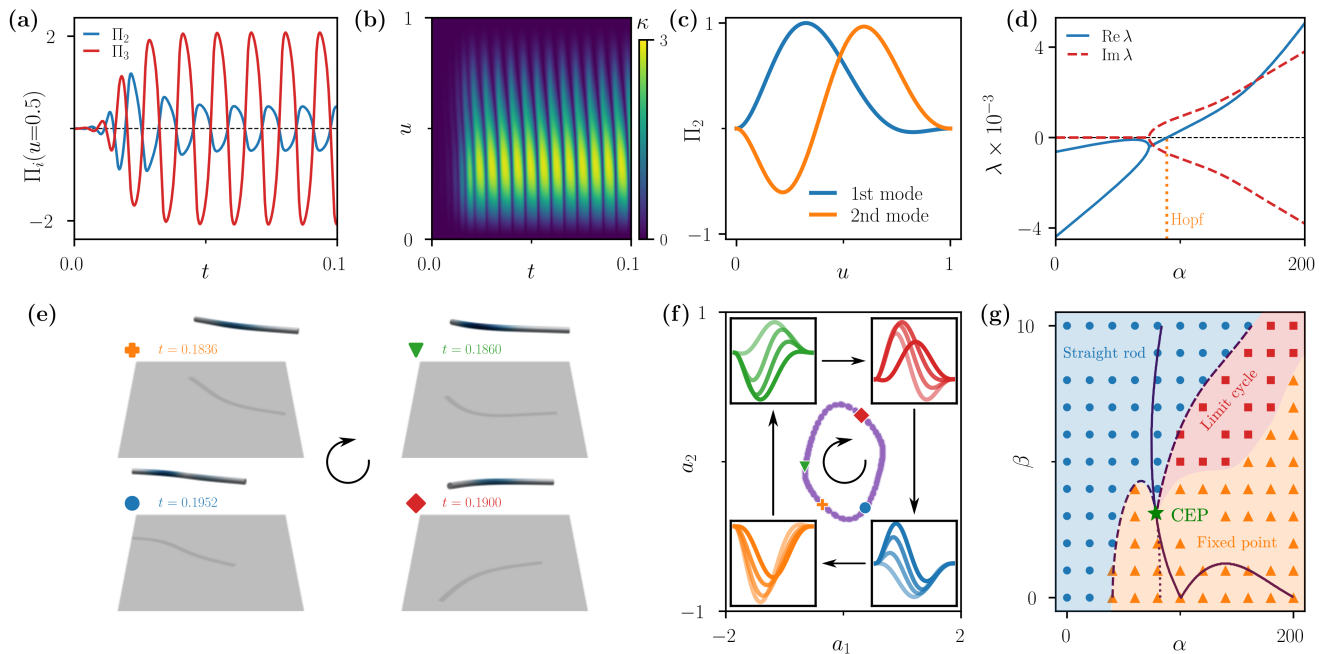


Figure 3. Curvature evolution of a polar, achiral rod with  $\alpha = 100, \beta = 5$ , exhibiting a limit cycle in shape space. (a) Temporal evolution of  $\Pi_2, \Pi_3$  the midpoint of the rod. (b) Curvature kymograph of the rod. (c) Dominant  $\Pi_2$  modes obtained from principal component analysis (PCA). (d) Real and imaginary parts of the leading two eigenvalues of the dynamics at  $\beta = 5$  as a function of  $\alpha$ . (e) Snapshots of the rod dynamics over a limit cycle. The rod is shaded according to its scalar curvature. The gray plane is a guide to the eye and does not represent a physical boundary. See Movie 2 of the SM [57] for animations of the limit cycle. (f)  $\Pi_2$  dynamics of the rod projected onto the subspace spanned by the two dominant PCA modes, exhibiting a limit cycle. The insets show the evolution of  $\Pi_2$  along the limit cycle. (g) Phase diagram of a polar, achiral rod. The dashed and dotted lines are the curves where the first and the second leading eigenvalues of the linearized dynamics cross the real axis, while the solid line is where they acquire an imaginary part. The intersection near  $\alpha \approx 77, \beta \approx 3$  of the three curves is a critical exceptional point. Crossing from the blue to the red region of the phase diagram upon increasing  $\alpha$ , we find a characteristic Hopf bifurcation. Reentrant behavior is observed for  $\beta \approx 4$ .

a periodic attractor in shape space, corresponding to a time-periodic deformation pattern involving coordinated oscillations of curvature modes along the filament, see Fig. 3(a)-(b).

The origin of this transition can be understood from the interplay of curvature production and transport. While the  $\alpha$  term promotes curvature generation, the polar coefficient  $\beta$  introduces advective coupling in the shape dynamics, producing an imaginary component in the spectrum of the linearized operator. Together with elastic relaxation, this provides a generic mechanism for oscillatory instability. Fig. 3(g) summarizes the resulting phase diagram. The Hopf bifurcation governs the onset of oscillations, while the intersection of instability boundaries near  $\alpha \approx 77, \beta \approx 3$  corresponds to a critical exceptional point [40, 61] where two eigenvalues simultaneously go to zero and the eigenspace becomes degenerate, with the three phases (straight rod, nontrivial fixed point, limit cycle) meeting there.

Upon reconstruction, periodic attractors in shape space correspond to autonomous swimming gaits in physical space, see Fig. 3(e). Each cycle in shape space pro-

duces a net displacement through the kinematic coupling between deformation and rigid motion, in analogy with the geometric phase underlying low-Reynolds-number locomotion [14, 62, 63]. Unlike classical geometric descriptions [64], however, the limit cycle is not prescribed but emerges dynamically through a bifurcation due to the nonreciprocity of the medium. The resulting motion is therefore an autonomous gait selected by the intrinsic shape dynamics. We note that left-right symmetry breaking is not essential: oscillatory attractors persist even in apolar, achiral rods at sufficiently large activity [57].

*Chaos (chaotic attractors).* Periodic attractors of RAD systems generically lose stability to chaotic attractors arising from the interaction of instability, transport, and dissipation. Further exploring the nonreciprocal parameter space, we identify a regime in which the shape dynamics of a polar, chiral rod ( $\beta, \delta \neq 0, \alpha = \epsilon = 0$ ) evolves onto a chaotic attractor, see Fig. 4. In this regime, the curvature field exhibits seemingly chaotic spatiotemporal structure, while projections onto the dominant principal components reveal an effective low-dimensional bounded

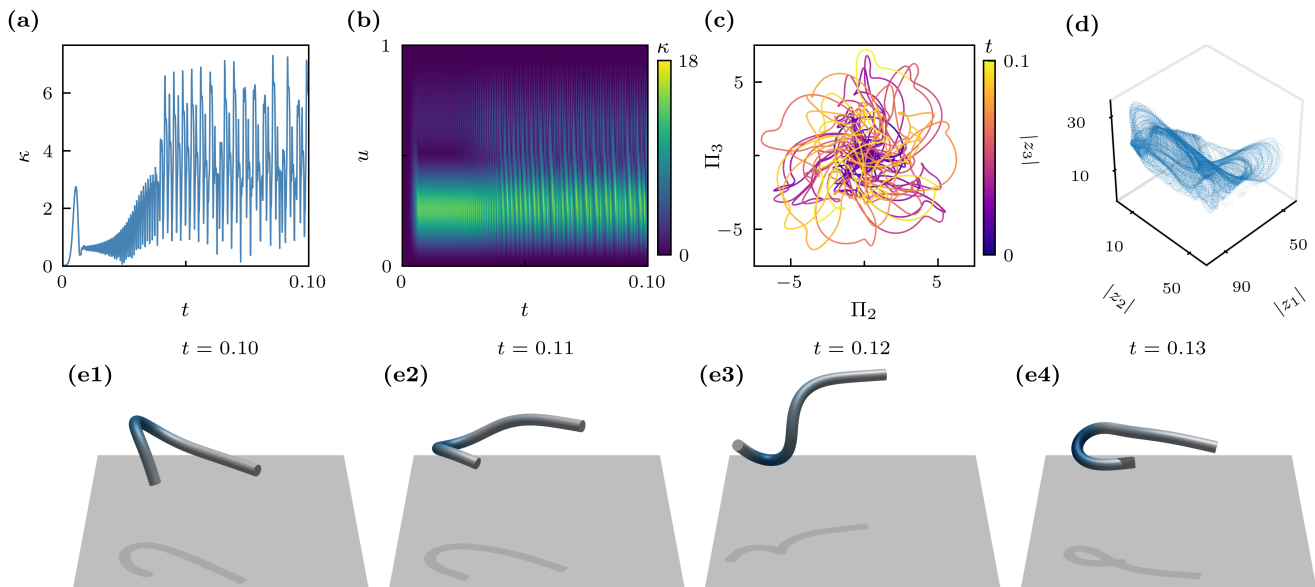


Figure 4. Chaotic dynamics for  $\delta = 15, \beta = 3.5$ . (a) Temporal evolution of the curvature of the midpoint of the rod. (b) Curvature kymograph of the rod. (c) Evolution of the shape of the rod at the midpoint in  $\Pi_2 - \Pi_3$  space. (d) Chaotic attractor formed from scatter plot of dynamics projected onto the amplitudes of the first three dominant eigenmodes obtained from PCA. (e1)–(e4) Snapshots of chaotic rod dynamics. See Movie 3 of the SM [57] for animations of chaotic dynamics.

chaotic trajectory in shape space.

The onset of chaos arises from the competing roles of the nonreciprocal contributions. The chiral coefficient  $\delta$  destabilizes the straight configuration and continuously injects curvature into the filament, while the polar coefficient  $\beta$  advects curvature fluctuations along its length. In a finite filament, these disturbances are repeatedly reflected at the free boundaries and interact nonlinearly with newly generated curvature waves. Upon reconstruction, chaotic attractors in shape space correspond to irregular trajectories in physical space, characterized by aperiodic sequences of bending, rotation, and writhing driven by the underlying deformation dynamics. The resulting motion is therefore neither steady nor periodic, but governed by chaotic evolution in shape space [65–67].

This mechanism closely parallels other pattern-forming systems exhibiting deterministic chaos, such as the Kuramoto–Sivashinsky equation [68, 69], where unstable long-wavelength modes are balanced by higher-order dissipation. Here, however, the chaotic dynamics unfolds in shape space and is mapped to physical motion through the kinematics.

*Discussion.* We have shown that the elasto-hydrodynamics of nonreciprocal slender solids admits a closed description in shape space, where Euclidean symmetry is factored out and deformation evolves as a nonlinear RAD system. This reformulates nonreciprocal active elasto-hydrodynamics as a pattern-formation problem: fixed points, limit cycles, and chaotic attractors of the shape dynamics manifest as rigid motion, autonomous swim-

ming gaits, and chaotic locomotion in physical space. In contrast to classical geometric theories of swimming, where shape changes are prescribed, the relevant trajectories in shape space emerge spontaneously through instabilities of the nonreciprocally active medium.

Although we focused on the simplest local nonreciprocal force and torque densities compatible with Euclidean invariance, the bifurcations reported here appear robust and show qualitative agreement with detailed hydrodynamic models of nonreciprocal active slender bodies [19, 21, 35]. This suggests that the observed phenomenology reflects generic dynamical structures of nonreciprocal slender bodies rather than specific constitutive choices. The appearance of Hopf bifurcations, chaos, and exceptional points further points to connections with pattern formation and non-Hermitian dynamics [70]. Bifurcations in shape space dynamics can be harnessed via spatiotemporal modulation of the nonreciprocal coefficients to control the shape and motion of nonreciprocal filaments [71].

The shape-space formulation also opens several analytical directions. Nonlocal hydrodynamic interactions and fluctuations can be incorporated systematically, while the reaction–advection–diffusion structure provides a natural starting point for amplitude-equation and normal-form descriptions near instability thresholds [52]. It may also offer a route toward connecting nonreciprocal filament dynamics with geometric evolution equations and classical theories of curve dynamics [72, 73].

*Acknowledgements.* We thank Anton Souslov, Brato Chakrabarti and Rajesh Singh for stimulating discussions

and helpful suggestions. This research was supported by Engineering and Physical Sciences Research Council Grant No. EP/W524141/1 (B.N.) and W108115D (M.W.) B.N. and M.W. contributed equally to this work.

*Data availability.* The data supporting the findings of this study are available within the article.

---

\* bn273@cam.ac.uk

† mrmaw2@cam.ac.uk

‡ ra413@cam.ac.uk

- [1] J. Gray and G. J. Hancock, The Propulsion of Sea-Urchin Spermatozoa, *Journal of Experimental Biology* **32**, 802 (1955).
- [2] B. Audoly and Y. Pomeau, eds., *Elasticity and geometry: from hair curls to the non-linear response of shells* (Oxford University Press, 2010).
- [3] B. Audoly and S. Neukirch, Fragmentation of Rods by Cascading Cracks: Why Spaghetti Does Not Break in Half, *Physical Review Letters* **95**, 095505 (2005).
- [4] W. F. Baker and A. McRobie, eds., *The Geometry of Equilibrium: James Clerk Maxwell and 21st-Century Structural Mechanics*, 1st ed. (Cambridge University Press, 2025).
- [5] L. Euler, *Methodus inveniendi lineas curvas maximi minive proprietate gaudentes* (Bousquet, Lausanne & Geneva, 1744).
- [6] G. Kirchhoff, Über das Gleichgewicht und die Bewegung eines unendlich dünnen elastischen Stabes, *Journal für die reine und angewandte Mathematik* **56**, 285 (1859).
- [7] S. Timoshenko, LXVI. On the correction for shear of the differential equation for transverse vibrations of prismatic bars, *The London, Edinburgh, and Dublin Philosophical Magazine and Journal of Science* **41**, 744 (1921).
- [8] J. L. Ericksen and C. Truesdell, Exact theory of stress and strain in rods and shells, *Archive for Rational Mechanics and Analysis* **1**, 295 (1957).
- [9] A. Goriely and M. Tabor, The Nonlinear Dynamics of Filaments, *Nonlinear Dynamics* **21**, 101 (2000).
- [10] S. Antman, *Nonlinear Problems of Elasticity* (Springer, New York, 2004).
- [11] D. E. Moulton, H. Oliveri, and A. Goriely, Multiscale integration of environmental stimuli in plant tropism produces complex behaviors, *Proceedings of the National Academy of Sciences* **117**, 32226 (2020).
- [12] P. Sartori, V. F. Geyer, J. Howard, and F. Jülicher, Curvature regulation of the ciliary beat through axonemal twist, *Physical Review E* **94**, 042426 (2016).
- [13] B. Chakrabarti and D. Saintillan, Spontaneous oscillations, beating patterns, and hydrodynamics of active microfilaments, *Physical Review Fluids* **4**, 043102 (2019).
- [14] J. M. Rieser, B. Chong, C. Gong, H. C. Astley, P. E. Schiebel, K. Diaz, C. J. Pierce, H. Lu, R. L. Hatton, H. Choset, and D. I. Goldman, Geometric phase predicts locomotion performance in undulating living systems across scales, *Proceedings of the National Academy of Sciences* **121**, e2320517121 (2024).
- [15] C. Kaeser, J. Kwon, E. Challita, H. Tuazon, R. J. Wood, S. Bhamla, and J. Werfel, Individual and Collective Behaviors in Soft Robot Worms Inspired by Living Worm Blobs, in *2025 IEEE International Conference on Robotics and Automation (ICRA)* (IEEE, Atlanta, GA, USA, 2025) pp. 2577–2583.
- [16] J. Lighthill, Flagellar Hydrodynamics, *SIAM Review* **18**, 161 (1976).
- [17] C. H. Wiggins and R. E. Goldstein, Flexive and Propulsive Dynamics of Elastica at Low Reynolds Number, *Physical Review Letters* **80**, 3879 (1998).
- [18] E. Lauga, Floppy swimming: Viscous locomotion of actuated elastica, *Physical Review E* **75**, 041916 (2007).
- [19] M. D. Butler, B. J. Walker, T. D. Montenegro-Johnson, and P. Katsamba, Elastohydrodynamics of three-dimensional chemically active filaments, *Journal of Fluid Mechanics* **1029**, A42 (2026).
- [20] M. C. Marchetti, J. F. Joanny, S. Ramaswamy, T. B. Liverpool, J. Prost, M. Rao, and R. A. Simha, Hydrodynamics of soft active matter, *Reviews of Modern Physics* **85**, 1143 (2013).
- [21] U. Makanga, A. Varma, and P. Katsamba, Instability and self-propulsion of flexible autophoretic filaments, *Physical Review Fluids* **11**, 053101 (2026).
- [22] A. Maitra and S. Ramaswamy, Oriented Active Solids, *Physical Review Letters* **123**, 238001 (2019).
- [23] F. Brauns, M. O’Leary, A. Hernandez, M. J. Bowick, and M. C. Marchetti, Active Solids: Topological Defect Self-Propulsion Without Flow, *Physical Review Letters* **136**, 058302 (2026).
- [24] J. Elgeti, R. G. Winkler, and G. Gompper, Physics of microswimmers—single particle motion and collective behavior: a review, *Reports on Progress in Physics* **78**, 056601 (2015).
- [25] T. Parthasarathy, F. K. Chan, and M. Gazzola, Streaming-enhanced flow-mediated transport, *Journal of Fluid Mechanics* **878**, 647 (2019).
- [26] T. Ranzani, M. Cianchetti, G. Gerboni, I. D. Falco, and A. Menciassi, A Soft Modular Manipulator for Minimally Invasive Surgery: Design and Characterization of a Single Module, *IEEE Transactions on Robotics* **32**, 187 (2016).
- [27] A. Tekinalp, N. Naughton, S. H. Kim, U. Halder, R. Gillette, P. G. Mehta, W. Kier, and M. Gazzola, Topology, dynamics, and control of a muscle-architected soft arm, *Proceedings of the National Academy of Sciences* **121**, e2318769121 (2024).
- [28] A. Gopal Subramaniam, M. Kumar, S. Thutupalli, and R. Singh, Rigid flocks, undulatory gaits, and chiral foldamers in a chemically active polymer, *New Journal of Physics* **26**, 083009 (2024).
- [29] X. Chao, K. Skipper, C. P. Royall, S. Henkes, and T. B. Liverpool, Traveling Strings of Active Dipolar Colloids, *Physical Review Letters* **134**, 018302 (2025).
- [30] M. Wei and D. J. Kraft, Life-like behavior emerging in active and flexible microstructures, *Proceedings of the National Academy of Sciences* **123**, e2531743123 (2026).
- [31] M. Brandenbourger, X. Locsin, E. Lerner, and C. Coulais, Non-reciprocal robotic metamaterials, *Nature Communications* **10**, 4608 (2019).
- [32] Y. Chen, X. Li, C. Scheibner, V. Vitelli, and G. Huang, Realization of active metamaterials with odd micropolar elasticity, *Nature Communications* **12**, 5935 (2021).
- [33] M. Gelvan, A. Chirko, J. Kirpich, Y. Lavie, N. Israel, and N. Oppenheimer, Hydrodynamic spin-pairing and active polymerization of oppositely spinning rotors, *Nature Communications* **16**, 10368 (2025).
- [34] J. Veenstra, C. Scheibner, M. Brandenbourger, J. Binysh, A. Souslov, V. Vitelli, and C. Coulais, Adaptive locomo-

- tion of active solids, *Nature* **639**, 935 (2025).
- [35] G. Jayaraman, S. Ramachandran, S. Ghose, A. Laskar, M. S. Bhamla, P. B. S. Kumar, and R. Adhikari, Autonomous Motility of Active Filaments due to Spontaneous Flow-Symmetry Breaking, *Physical Review Letters* **109**, 158302 (2012).
- [36] R. G. Winkler and G. Gompper, The physics of active polymers and filaments, *The Journal of Chemical Physics* **153**, 040901 (2020).
- [37] K. R. Prathyusha, F. Ziebert, and R. Golestanian, Emergent conformational properties of end-tailored transversely propelling polymers, *Soft Matter* **18**, 2928 (2022).
- [38] W. Lough, D. B. Weibel, and S. E. Spagnolie, Self-buckling and self-writhing of semi-flexible microorganisms, *Soft Matter* **19**, 7349 (2023).
- [39] C. Scheibner, A. Souslov, D. Banerjee, P. Surówka, W. T. M. Irvine, and V. Vitelli, Odd elasticity, *Nature Physics* **16**, 475 (2020).
- [40] S. C. Al-Izzi, Y. Du, J. Veenstra, R. G. Morris, A. Souslov, A. Carlson, C. Coulais, and J. Binysh, Nonreciprocal buckling makes active filaments polyfunctional, *Proceedings of the National Academy of Sciences* **123**, e2531723123 (2026).
- [41] K. Ishimoto, C. Moreau, and K. Yasuda, Self-organized swimming with odd elasticity, *Physical Review E* **105**, 064603 (2022).
- [42] G. De Canio, E. Lauga, and R. E. Goldstein, Spontaneous oscillations of elastic filaments induced by molecular motors, *Journal of The Royal Society Interface* **14**, 20170491 (2017).
- [43] F. Ling, H. Guo, and E. Kanso, Instability-driven oscillations of elastic microfilaments, *Journal of The Royal Society Interface* **15**, 20180594 (2018).
- [44] B. Clarke, Y. Hwang, and E. E. Keaveny, Bifurcations and nonlinear dynamics of the follower force model for active filaments, *Physical Review Fluids* **9**, 073101 (2024).
- [45] M. Warda and R. Adhikari, Elastohydrodynamic instabilities of a soft robotic arm in a viscous fluid, *Physical Review Research* **8**, 013229 (2026).
- [46] J. J. Blum and M. Hines, Biophysics of flagellar motility, *Quarterly Reviews of Biophysics* **12**, 103 (1979).
- [47] D. Mondal, R. Adhikari, and P. Sharma, Internal friction controls active ciliary oscillations near the instability threshold, *Science Advances* **6**, eabb0503 (2020).
- [48] A. Poncet and D. Bartolo, When Soft Crystals Defy Newton's Third Law: Nonreciprocal Mechanics and Dislocation Motility, *Physical Review Letters* **128**, 048002 (2022).
- [49] B. Németh, T. Kobayashi, and R. Adhikari, Nonreciprocal constitutive laws for oriented active solids, *New Journal of Physics* **28**, 034401 (2026).
- [50] R. E. Goldstein and S. A. Langer, Nonlinear Dynamics of Stiff Polymers, *Physical Review Letters* **75**, 1094 (1995).
- [51] J. F. Cass and H. Bloomfield-Gadélha, The reaction-diffusion basis of animated patterns in eukaryotic flagella, *Nature Communications* **14**, 5638 (2023).
- [52] M. C. Cross and P. C. Hohenberg, Pattern formation outside of equilibrium, *Reviews of Modern Physics* **65**, 851 (1993).
- [53] M. Cross and H. Greenside, *Pattern Formation and Dynamics in Nonequilibrium Systems*, 1st ed. (Cambridge University Press, 2009).
- [54] M. Garg and A. Kumar, A slender body theory for the motion of special Cosserat filaments in Stokes flow, *Mathematics and Mechanics of Solids* **28**, 692 (2023).
- [55] R. Aditi Simha and S. Ramaswamy, Hydrodynamic Fluctuations and Instabilities in Ordered Suspensions of Self-Propelled Particles, *Physical Review Letters* **89**, 058101 (2002).
- [56] G. P. Alexander, S. J. Kole, A. Maitra, and S. Ramaswamy, Screw symmetry, chiral hydrodynamics, and odd instability in active cholesterics, *Physical Review E* **112**, 055424 (2025).
- [57] See supplemental material at [url will be inserted by publisher] for animations of rod dynamics and derivations of equations, which includes ref. [74].
- [58] M. Kumar, A. Murali, A. G. Subramaniam, R. Singh, and S. Thutupalli, Emergent dynamics due to chemohydrodynamic self-interactions in active polymers, *Nature Communications* **15**, 4903 (2024).
- [59] L. D. Landau, L. P. Pitaevskii, E. M. Lifshitz, and A. M. Kosevich, *Theory of elasticity*, 3rd ed. (Butterworth-Heinemann, Oxford, England, 1984).
- [60] R. E. Goldstein, T. R. Powers, and C. H. Wiggins, Viscous Nonlinear Dynamics of Twist and Writhe, *Physical Review Letters* **80**, 5232 (1998).
- [61] M. Fruchart, R. Hanai, P. B. Littlewood, and V. Vitelli, Non-reciprocal phase transitions, *Nature* **592**, 363 (2021).
- [62] A. Shapere and F. Wilczek, Geometry of self-propulsion at low Reynolds number, *Journal of Fluid Mechanics* **198**, 557 (1989).
- [63] E. Kanso, Swimming due to transverse shape deformations, *Journal of Fluid Mechanics* **631**, 127 (2009).
- [64] R. Montgomery, Gauge Theory of the Falling Cat, in *Dynamics and Control of Mechanical Systems*, edited by M. Enos (American Mathematical Society, 1993) pp. 193–218.
- [65] D. Krishnamurthy and M. Prakash, Emergent programmable behavior and chaos in dynamically driven active filaments, *Proceedings of the National Academy of Sciences* **120**, e2304981120 (2023).
- [66] S. Sarkar, B. Ash, Y. Wu, N. Boechler, S. Shankar, and X. Mao, Mechanochemical Feedback Drives Complex Inertial Dynamics in Active Solids, *Physical Review Letters* **135**, 258301 (2025).
- [67] F. Bonacci, B. Chakrabarti, O. d. Roure, A. Lindner, and D. Saintillan, Reversibility, Chaos, and Attractors in Periodically Sheared Elastic Filaments (2026), arXiv:2601.00643 [cond-mat.soft].
- [68] Y. Kuramoto and T. Tsuzuki, Persistent Propagation of Concentration Waves in Dissipative Media Far from Thermal Equilibrium, *Progress of Theoretical Physics* **55**, 356 (1976).
- [69] G. Sivashinsky, Nonlinear analysis of hydrodynamic instability in laminar flames—I. Derivation of basic equations, *Acta Astronautica* **4**, 1177 (1977).
- [70] Y. Ashida, Z. Gong, and M. Ueda, Non-Hermitian physics, *Advances in Physics* **69**, 249 (2020).
- [71] L. Qiao and R. Kapral, Control of Active Polymeric Filaments by Chemically Powered Nanomotors, *Physical Review Applied* **18**, 024051 (2022).
- [72] H. Hasimoto, A soliton on a vortex filament, *Journal of Fluid Mechanics* **51**, 477 (1972).
- [73] A. E. Cohen, A. D. Hastewell, S. Pradhan, S. W. Flavell, and J. Dunkel, Schrödinger Dynamics and Berry Phase of Undulatory Locomotion, *Physical Review Letters* **130**, 258402 (2023).

[74] A. Müller, Review of the exponential and Cayley map on SE(3) as relevant for Lie group integration of the generalized Poisson equation and flexible multibody systems,

Proceedings of the Royal Society A: Mathematical, Physical and Engineering Sciences **477**, 20210303 (2021).

## SUPPLEMENTARY MATERIAL

### I. GEOMETRIC FLOW AND SHAPE SPACE EQUATIONS

In this section, we give the explicit form of the equations of motion studied in the Letter. For this, it is useful to introduce the covariant derivative operator

$$D = \partial_u + \underline{\Pi} \times . \quad (\text{S9})$$

Combining Eqs. (3) and (4) of the main text, we obtain

$$\begin{aligned} \dot{\underline{h}} &= \frac{1}{\gamma^T} D (D\underline{F} + \underline{f}) + \frac{1}{\gamma^R} \underline{h} \times (D\underline{M} + \underline{h} \times \underline{F} + \underline{m}), \\ \dot{\underline{\Pi}} &= \frac{1}{\gamma^R} D (D\underline{M} + \underline{h} \times \underline{F} + \underline{m}). \end{aligned} \quad (\text{S10})$$

We close the equations by substituting the constitutive laws for the contact forces and moments

$$\underline{F} = \underline{k}^T (\underline{h} - \underline{e}_1), \quad \underline{M} = \underline{k}^R \underline{\Pi}, \quad (\text{S11})$$

as well as the active force and torque densities

$$\underline{f} = \underline{e}_1 \times (\alpha \underline{\Pi} + \epsilon \underline{\Pi} \times \underline{e}_1), \quad \underline{m} = \underline{e}_1 \times (\delta \underline{\Pi} + \beta \underline{\Pi} \times \underline{e}_1). \quad (\text{S12})$$

We find

$$\begin{aligned} \dot{\underline{h}} &= \frac{1}{\gamma^T} \left( D^2 \underline{k}^T [\underline{h} - \underline{e}_1] + D [e_1 \times (\alpha \underline{\Pi} + \epsilon \underline{\Pi} \times \underline{e}_1)] \right) \\ &\quad + \frac{1}{\gamma^R} \underline{h} \times \left( D \underline{k}^R \underline{\Pi} + \underline{h} \times \underline{k}^T [\underline{h} - \underline{e}_1] + \underline{e}_1 \times [\delta \underline{\Pi} + \beta \underline{\Pi} \times \underline{e}_1] \right) \\ \dot{\underline{\Pi}} &= \frac{1}{\gamma^R} \left( D^2 \underline{k}^R \underline{\Pi} + D [\underline{h} \times \underline{k}^T (\underline{h} - \underline{e}_1)] + D [e_1 \times (\delta \underline{\Pi} + \beta \underline{\Pi} \times \underline{e}_1)] \right) \end{aligned} \quad (\text{S13})$$

The stress-free boundary conditions imply that  $\underline{h} = \underline{e}_1$  and  $\underline{\Pi} = 0$  at  $u = 0, L$  at all times, so that the boundary conditions are

$$h_1 = 1, h_2 = h_3 = 0, \quad \Pi_1 = \Pi_2 = \Pi_3 = 0 \quad (\text{S14})$$

at both end points of the rod.

### II. LINEARIZED GEOMETRIC FLOW ON SLOW MANIFOLD

We linearize the governing equations of our theory, namely Eqs. (3) and (4) of the main text as follows. The governing equations are closed by specifying the constitutive laws  $\underline{F} = \underline{k}^T (\underline{h} - \underline{e}_1)$  and  $\underline{M} = \underline{k}^R \underline{\Pi}$  and the moving frame components of the active force and torque densities

$$\begin{aligned} \underline{f} &= \alpha \begin{bmatrix} 0 \\ -\Pi_3 \\ \Pi_2 \end{bmatrix} + \epsilon \begin{bmatrix} 0 \\ \Pi_2 \\ \Pi_3 \end{bmatrix}, \\ \underline{m} &= \delta \begin{bmatrix} 0 \\ -\Pi_3 \\ \Pi_2 \end{bmatrix} + \beta \begin{bmatrix} 0 \\ \Pi_2 \\ \Pi_3 \end{bmatrix}. \end{aligned} \quad (\text{S15})$$

We linearize the equations about the stationary, straight reference configuration

$$\left(\underline{h}^{(0)}, \underline{\Pi}^{(0)}\right) = \left(\underline{e}_1, \underline{0}\right), \quad \left(\underline{v}^{(0)}, \underline{\Omega}^{(0)}\right) = \left(\underline{0}, \underline{0}\right). \quad (\text{S16})$$

The linearized compatibility equations are

$$\dot{\underline{h}} = \underline{v}' - \underline{\Omega} \times \underline{e}_1, \quad \dot{\underline{\Pi}} = \underline{\Omega}'. \quad (\text{S17})$$

We kinematically eliminate the shear, stretch, and twist degrees of freedom by imposing  $\underline{h} = 0$  and  $\Pi_1 = 0$ , through which we obtain  $\Omega_3 = v_2'$ ,  $\Omega_2 = -v_3'$ , and subsequently

$$\dot{\Pi}_2 = -v_3'', \quad \dot{\Pi}_3 = v_2''. \quad (\text{S18})$$

On the other hand, linearizing the force and torque balance in the filament limit gives

$$\gamma^T \underline{v} = \underline{F}' + \underline{f}, \quad \underline{0} = \underline{M}' + \underline{e}_1 \times \underline{F} + \underline{m}. \quad (\text{S19})$$

Substituting the constitutive equations into the linearized torque balance, differentiating once, and combining the result with the linearized force balance yields

$$\begin{aligned} \gamma^T v_2 &= -k_{\perp}^R \Pi_3'' - \beta \Pi_3' - \alpha \Pi_3 - \delta \Pi_2' + \epsilon \Pi_2, \\ \gamma^T v_3 &= k_{\perp}^R \Pi_2'' + \beta \Pi_2' + \alpha \Pi_2 - \delta \Pi_3' + \epsilon \Pi_3. \end{aligned} \quad (\text{S20})$$

We obtain a closed linear system in terms of the perturbations to the curvature,  $\Pi_2$  and  $\Pi_3$ , by differentiating (S19) twice and substituting the resulting equations into (S18). Introducing the complex-valued curvature  $\Pi \equiv \Pi_2 + i\Pi_3$ , we may compactly write the resulting linear system as

$$\gamma^T \dot{\Pi} = -k_{\perp}^R \Pi'''' - (\beta + i\delta) \Pi''' - (\alpha - i\epsilon) \Pi''. \quad (\text{S21})$$

After nondimensionalization, we may write the dimensionless form of the linear system as

$$\dot{\Pi} = -\Pi'''' - \mu \Pi''' - \nu \Pi'', \quad (\text{S22})$$

and  $\mu = (\beta + i\delta) \times L/k_{\perp}^R$ ,  $\nu = (\alpha - i\epsilon) \times L^2/k_{\perp}^R$  are nondimensional complex-valued activity parameters. The free-free boundary conditions on the fully nonlinear system translate to the following boundary conditions on the linear system (S22). Imposing the zero torque boundary conditions  $M_2 = M_3 = 0$  at  $u = 0, L$  implies that  $\Pi = 0$  at  $u = 0, L$ . On the other hand, using the linearized equation  $0 = \underline{M}' + \underline{e}_1 \times \underline{F} + \underline{m}$ , we find that at  $u = 0, L$

$$F_2 = -k_{\perp}^R \Pi_3', \quad F_3 = k_{\perp}^R \Pi_2'. \quad (\text{S23})$$

Thus, imposing the zero force boundary conditions  $F_2 = F_3 = 0$  at  $u = 0, L$  implies that  $\Pi' = 0$  at  $u = 0, L$ .

### III. LINEAR STABILITY ANALYSIS

In this section, we investigate the behavior of the linearized dynamics

$$\dot{\Pi} = -\Pi'''' - \mu \Pi''' - \nu \Pi'', \quad (\text{S24})$$

in terms of the nondimensionalized complex curvature  $\Pi = \Pi_2 + i\Pi_3$ , where  $\mu = (\beta + i\delta) \times L/k_{\perp}^R$ ,  $\nu = (\alpha - i\epsilon) \times L^2/k_{\perp}^R$  are nondimensional complex-valued activity parameters, with boundary conditions  $\Pi = \Pi' = 0$  at  $u = 0, 1$ . With a slight abuse of notation, we shall use  $\alpha, \beta, \delta, \epsilon$  for the nondimensionalized active moduli too.

We are interested in the spectrum of the differential operator

$$\mathcal{L} = -\frac{d^4}{du^4} - \mu \frac{d^3}{du^3} - \nu \frac{d^2}{du^2} \quad (\text{S25})$$

equipped with the boundary conditions

$$\Pi(0) = \Pi'(0) = \Pi(1) = \Pi'(1) = 0. \quad (\text{S26})$$

We equip the space of complex-valued functions on  $[0, 1]$  with the standard  $L^2$  inner product

$$(f, g) = \int_0^1 f(u)^* g(u) du. \quad (\text{S27})$$

With respect to the inner product (S27), we find, after repeated integrations by parts, that

$$(f, \mathcal{L}g) = (\mathcal{L}^\dagger f, g) \quad (\text{S28})$$

where

$$\mathcal{L}^\dagger = -\frac{d^4}{du^4} + \mu^* \frac{d^3}{du^3} - \nu^* \frac{d^2}{du^2}, \quad (\text{S29})$$

from which we conclude the following:

- The **apolar, achiral** operator

$$\mathcal{L}_{\text{AP}}^{\text{AC}} = -\frac{d^4}{du^4} - \alpha \frac{d^2}{du^2} \quad (\text{S30})$$

is Hermitian.

- The **apolar, chiral** operator

$$\mathcal{L}_{\text{AP}}^{\text{C}} = -\frac{d^4}{du^4} - i\delta \frac{d^3}{du^3} \quad (\text{S31})$$

is Hermitian.

- The **polar, achiral** operator

$$\mathcal{L}_{\text{P}}^{\text{AC}} = -\frac{d^4}{du^4} - \beta \frac{d^3}{du^3} \quad (\text{S32})$$

is non-Hermitian.

- The **polar, chiral** operator

$$\mathcal{L}_{\text{P}}^{\text{C}} = -\frac{d^4}{du^4} + i\epsilon \frac{d^2}{du^2} \quad (\text{S33})$$

is non-Hermitian.

We look for separable solutions of the form  $\Pi(t, u) = \Pi_n(u) e^{\zeta_n t}$ , leading to the following eigenvalue problem:

$$\Pi_n'''' + \mu \Pi_n'''' + \nu \Pi_n'' = -\zeta_n \Pi_n \quad (\text{S34})$$

with boundary conditions  $\Pi_n(0) = \Pi_n'(0) = \Pi_n(1) = \Pi_n'(1) = 0$ . Below, we will be interested in values of  $\mu, \nu$  where various eigenvalues  $\zeta_n$  cross the real axis, as this signals the  $n$ th mode becoming unstable. In particular, below we consider an apolar, achiral rod and an apolar, chiral rod, both of which have Hermitian linearized dynamics as shown above. Thus, both operators carry real eigenvalues  $\zeta_n \in \mathbb{R}$ .

### A. Apolar, achiral rod

In this subsection, we study a rod which has only  $\alpha$  nonzero and look for positive values of  $\alpha$  such that  $\zeta_n = 0$ . (Negative  $\alpha$  is an extra line tension and further stabilizes the straight configuration.) Eq. (S34) becomes:

$$\Pi_n'''' + \alpha \Pi_n'' = 0. \quad (\text{S35})$$

Let  $\xi = \sqrt{\alpha}$ . The boundary value problem (S35) has general solution

$$\Pi_n(u) = A \sin \xi u + B \cos \xi u + Cu + D$$

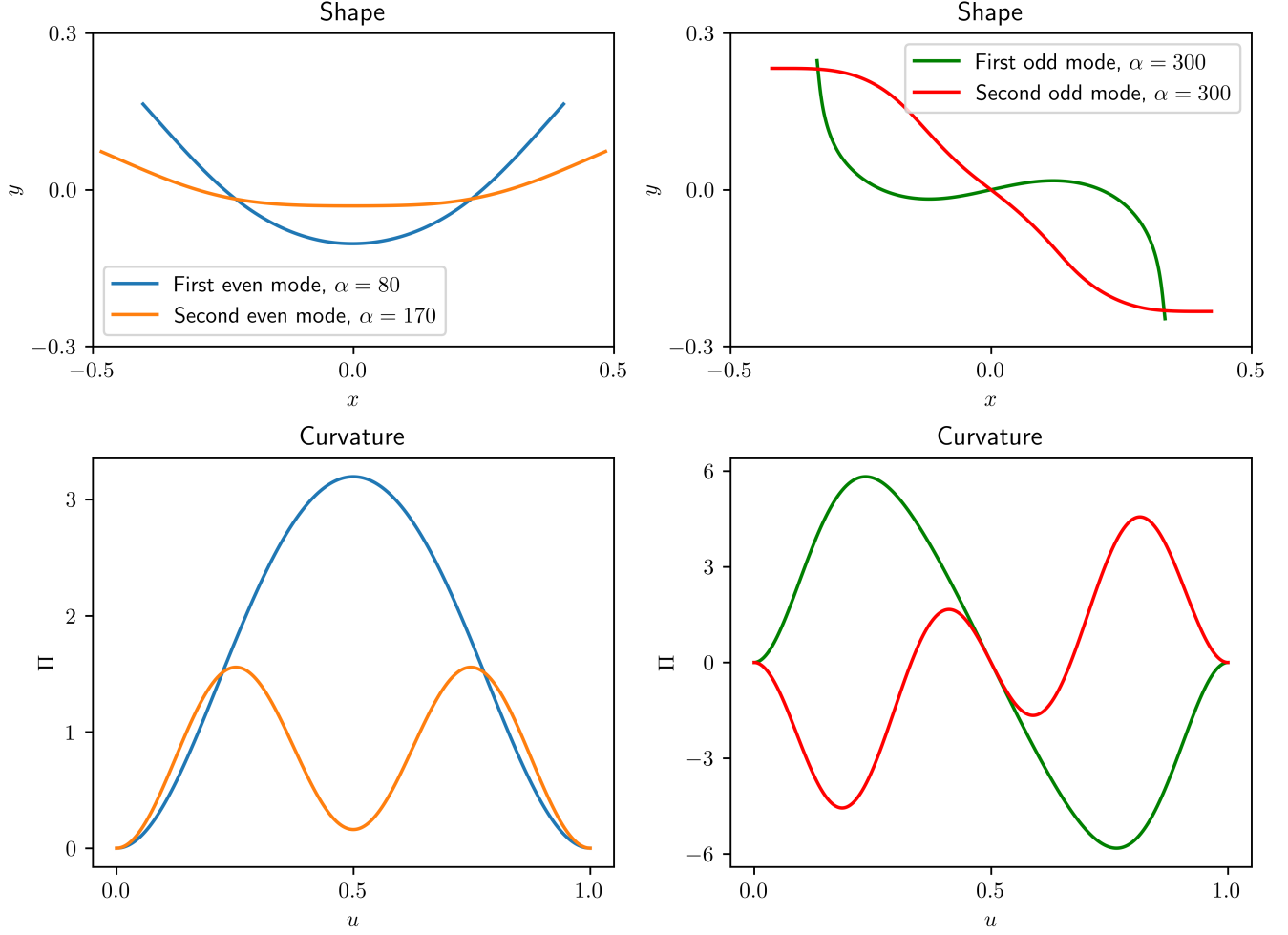


Figure S5. Dominant stationary curvature profiles and shapes obtained from linear stability analysis. Even modes correspond to  $\alpha_n = 4\pi n^2$ , while odd modes come from solutions of  $\frac{\alpha}{2} = \tan \frac{\alpha}{2}$ . By symmetry, even modes can only translate with a constant velocity, while odd modes rotate about their geometric center. Shapes were computed by solving the BVP Eq. (S35) using the routine `solve_bvp` in `scipy`.

for  $A, B, C, D$  constants. The boundary conditions lead to the following system of equations:

$$\begin{aligned} B + D &= 0, \\ \xi A + C &= 0, \\ A \sin \xi + B \cos \xi + C + D &= 0, \\ A \xi \cos \xi - B \xi \sin \xi + C &= 0. \end{aligned}$$

Eliminating  $C, D$  using the first two equations we get  $B = -D, C = -\xi A$ . Substituting these into the last two equations we find

$$\begin{pmatrix} \sin \xi - \xi & \cos \xi - 1 \\ \xi (\cos \xi - 1) & -\xi \sin \xi \end{pmatrix} \begin{pmatrix} A \\ B \end{pmatrix} = \begin{pmatrix} 0 \\ 0 \end{pmatrix}.$$

This system has a nonzero solution provided that the determinant vanishes, which, after some algebra, gives

$$2\xi \sin \frac{\xi}{2} \left( 2 \sin \frac{\xi}{2} - \xi \cos \frac{\xi}{2} \right) = 0.$$

As  $\xi > 0$ , we get two branches: either  $\sin \frac{\xi}{2} = 0$ , giving  $\xi_n = 2\pi n$  and  $\alpha_n = 4\pi^2 n^2$  for  $n > 1$  integer with a curvature profile  $\Pi(u) \propto 1 - \cos 2\pi n u$  corresponding to an even, self-propelling shape, or  $\frac{\xi}{2} = \tan \frac{\xi}{2}$ , which has no closed form

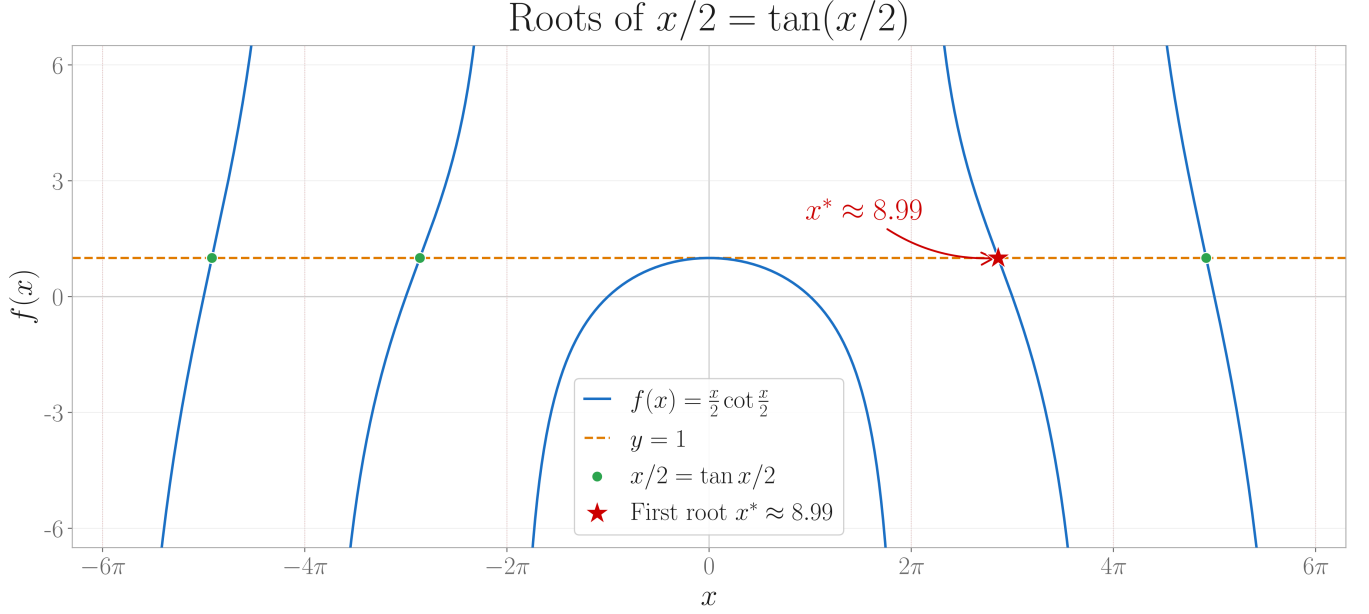


Figure S6. Roots of the transcendental equation  $\frac{\xi}{2} = \tan \frac{\xi}{2}$ .

solution, but its first nonzero root is roughly  $\xi \approx 9$ , and the curvature profile is

$$\Pi(u) \propto \frac{\sin\left(\xi\left(u - \frac{1}{2}\right)\right)}{\cos \frac{\xi}{2}} - \xi\left(u - \frac{1}{2}\right),$$

corresponding to a rotating  $S$ -shape. The  $U$ -shape first appears at  $\alpha_1 = 4\pi^2 \approx 40$ , consistently with simulations, while the  $S$ -shape only shows up at  $\alpha \approx 80$ , and is typically metastable.

### B. Apolar, chiral rod.

In this subsection, we look at a rod which has only  $\delta$  nonzero and look for values of  $\delta$  such that  $\zeta_n = 0$ . Eq. (S34) becomes:

$$\Pi_n'''' + i\delta\Pi_n''' = 0. \quad (\text{S36})$$

The boundary value problem (S36) has general solution

$$\Pi_n(u) = Ae^{-i\delta u} + Bu^2 + Cu + D \quad (\text{S37})$$

for constants  $A, B, C, D$ . The boundary conditions lead to the following system of equations:

$$\begin{aligned} A + D &= 0, \\ -i\delta A + C &= 0, \\ Ae^{-i\delta} + B + C + D &= 0, \\ -i\delta Ae^{-i\delta} + 2B + C &= 0. \end{aligned}$$

Eliminating  $C, D$  using the first two equations we get  $D = -A, C = i\delta A$ . Substituting these into the last two equations we find

$$\begin{pmatrix} e^{-i\delta} - 1 + i\delta & 1 \\ -i\delta(e^{-i\delta} - 1) & 2 \end{pmatrix} \begin{pmatrix} A \\ B \end{pmatrix} = \begin{pmatrix} 0 \\ 0 \end{pmatrix}.$$

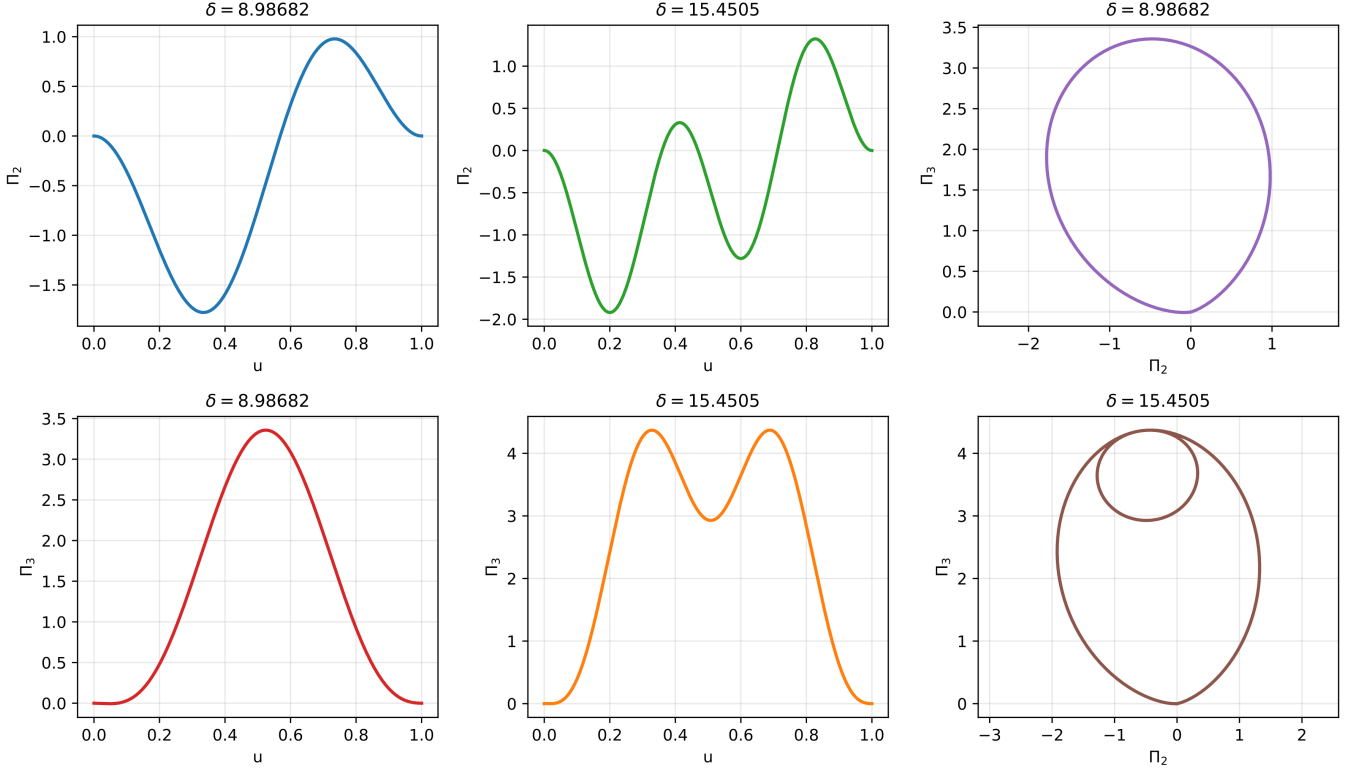


Figure S7. First two nonzero solutions to the boundary value problem (S36).

This system has a nonzero solution provided that the determinant vanishes, which, after some algebra, gives

$$\frac{\delta}{2} = \tan \frac{\delta}{2}.$$

The rod becomes unstable at the first nonzero root  $\delta = \pm\delta_c \approx \pm 8.99$  of this transcendental equation, irrespective of the sign of  $\delta$ .

#### IV. SELF-PROPULSION SPEED AT FIXED POINTS

##### A. Self-propelling U-shape

We look for translating solutions of the equations of motion, assuming a planar ( $h_3 = \Pi_1 = \Pi_2 = 0$ ) self-propelling U-shape:

$$\mathbf{v} = (\mathbf{F} - \alpha \mathbf{e}_1)'. \quad (\text{S38})$$

In Eq. (S38)  $\mathbf{v}$  is a constant vector. Integrating (S38) over the spatial extent of the rod and using the boundary conditions  $\mathbf{F} = \mathbf{0}$  gives:

$$\mathbf{v} = -\alpha [\mathbf{e}_1(1) - \mathbf{e}_1(0)]. \quad (\text{S39})$$

Let  $\mathbf{e}_1(u) = (\cos \theta(u), \sin \theta(u))$  for a scalar function  $\theta(u)$ , which we can take – by choosing our coordinate system appropriately – to satisfy  $\theta(1/2) = 0$ . Substituting this relation into (S39) we find:

$$\mathbf{v} = -\alpha (\cos \theta(1) - \cos \theta(0), \sin \theta(1) - \sin \theta(0)).$$

Since we have an even shape and curvature profile,  $\theta$  must be odd about  $u = 1/2$ , therefore the  $x$ -component of the self-propulsion vector is going to be zero, consistently with the symmetry of the shape. The  $y$ -component can be

simplified as  $\theta(1) = -\theta(0)$  and  $\Pi_3 = -\theta'$  to find:

$$\mathbf{v} = \alpha \left( 0, \sin \left[ \int_{1/2}^1 \Pi_3 du \right] - \sin \left[ \int_{1/2}^0 \Pi_3 du \right] \right).$$

Taking the modulus of both sides, we find the following simple result for the modulus  $v = |\mathbf{v}|$  of the self-propulsion velocity:

$$v = 2\alpha \sin \left( \frac{1}{2} \int_0^1 \Pi_3 du \right), \quad (\text{S40})$$

which is Eq. (8) of the main text.

## V. WEAKLY NONLINEAR ANALYSIS

### A. U-shape

We look for translating solutions of the equations of motion, assuming a planar shape:

$$\begin{aligned} \mathbf{v} &= (\mathbf{F} - \alpha \mathbf{e}_1)', \\ 0 &= \Pi_3' + h_1 F_2 - h_2 F_1. \end{aligned}$$

We work in the filament limit where  $h_1 = 1, h_2 = 0$  and  $F_1, F_2$  are Lagrange multipliers enforcing these constraints. Differentiating the first equation once again, we find:

$$\mathbf{F}'' = \alpha \mathbf{e}_1''$$

Expanding this equation in the moving frame, we get

$$\begin{aligned} (\underline{F}' + \underline{\Pi} \times \underline{F})' + \underline{\Pi} \times (\underline{F}' + \underline{\Pi} \times \underline{F}) &= \alpha (\underline{\Pi}' \times \underline{e}_1 + \underline{\Pi} \times (\underline{\Pi} \times \underline{e}_1)) \\ \underline{F}'' + 2\underline{\Pi} \times \underline{F}' + \underline{\Pi}' \times \underline{F} + \underline{\Pi} \times (\underline{\Pi} \times \underline{F}) &= \alpha (\underline{\Pi}' \times \underline{e}_1 + \underline{\Pi} \times (\underline{\Pi} \times \underline{e}_1)) \end{aligned}$$

The component-wise equations read:

$$\begin{aligned} F_1'' - 2\Pi_3 F_2' - F_2 \Pi_3' + (\alpha - F_1) \Pi_3^2 &= 0, \\ F_2'' + 2\Pi_3 F_1' - F_2 \Pi_3^2 - (\alpha - F_1) \Pi_3' &= 0, \\ \Pi_3' + F_2 &= 0. \end{aligned} \quad (\text{S41})$$

The boundary conditions are  $F_1 = F_2 = \Pi_3 = 0$  on both endpoints. We can eliminate  $F_2$  using the third equation:

$$\begin{aligned} F_1'' + 2\Pi_3 \Pi_3'' + (\Pi_3')^2 + (\alpha - F_1) \Pi_3^2 &= 0 \\ \Pi_3''' - 2\Pi_3 F_1' - \Pi_3^2 \Pi_3' + (\alpha - F_1) \Pi_3' &= 0 \end{aligned} \quad (\text{S42})$$

The boundary conditions become  $F_1 = \Pi_3 = \Pi_3' = 0$  on both endpoints. To ease notation, we will drop the indices from  $F_1, \Pi_3$  below.

We perform a weakly nonlinear analysis near the instability threshold  $\alpha_c = 4\pi^2$ . Let  $\alpha = \alpha_c + \varepsilon^2 \Delta$  and expand:

$$\begin{aligned} F &= \varepsilon F^{(1)} + \varepsilon^2 F^{(2)} + \varepsilon^3 F^{(3)} + \dots, \\ \Pi &= \varepsilon \Pi^{(1)} + \varepsilon^2 \Pi^{(2)} + \varepsilon^3 \Pi^{(3)} + \dots \end{aligned}$$

At linear order we get

$$\begin{aligned} F^{(1)''} &= 0, \\ \Pi^{(1)'''} + 4\pi^2 \Pi^{(1)'} &= 0. \end{aligned}$$

From the first equation, we get  $F^{(1)} = 0$ , while the second equation gives  $\Pi^{(1)} = A(1 - \cos(2\pi u))$ .

At quadratic order:

$$\begin{aligned} F^{(2)''} + 2\Pi^{(1)}\Pi^{(1)''} + (\Pi^{(1)'})^2 + 4\pi^2(\Pi^{(1)})^2 &= 0 \\ \Pi^{(2)''''} + 4\pi^2\Pi^{(2)'} &= 0 \end{aligned} \quad (\text{S43})$$

The first equation can be simplified to:

$$F^{(2)''} = 4\pi^2 A^2 (\cos(4\pi u) - 1) \quad (\text{S44})$$

Integrating it twice and applying the boundary conditions gives:

$$F^{(2)}(u) = A^2 \left[ 2\pi^2 u(1-u) + \frac{1 - \cos(4\pi u)}{4} \right] \quad (\text{S45})$$

At quadratic order,  $\Pi^{(2)}(u) = 0$  without loss of generality.

At cubic order, we get:

$$\begin{aligned} F^{(3)''} &= 0, \\ \Pi^{(3)''''} + 4\pi^2\Pi^{(3)'} &= 2\pi A \left( F^{(2)} - \Delta + A^2(1 - \cos(2\pi u))^2 \right) \sin(2\pi u) + 2A(1 - \cos(2\pi u)) F^{(2)'}. \end{aligned}$$

The amplitude equation for  $A$  follows from requiring the forcing on the RHS of the second equation to have no resonant term:

$$\int_0^1 \left\{ 2\pi A \left( F^{(2)} - \Delta + A^2(1 - \cos(2\pi u))^2 \right) \sin^2(2\pi u) + 2A(1 - \cos(2\pi u)) \sin 2\pi u F^{(2)'} \right\} du = 0.$$

Carrying out the integral, we find the amplitude equation

$$\left( \frac{35\pi}{8} + \frac{\pi^3}{3} \right) A^3 - \pi\Delta A = 0 \quad (\text{S46})$$

The amplitude equation admits the nontrivial steady-state solutions

$$A = \pm \sqrt{\frac{\Delta}{\frac{35}{8} + \frac{\pi^2}{3}}}. \quad (\text{S47})$$

Since the cubic coefficient  $\frac{35\pi}{8} + \frac{\pi^3}{3}$  is positive, nonzero solutions exist only for  $\Delta > 0$ , i.e. for  $(\alpha > \alpha_c)$ . The amplitude therefore scales as

$$A \propto \sqrt{\alpha - \alpha_c} \quad (\text{S48})$$

which is the characteristic scaling of a supercritical pitchfork bifurcation. Thus, the straight configuration loses stability continuously at  $\alpha = \alpha_c$ , giving rise to a branch of stable U-shaped translating solutions of arbitrarily small amplitude.

To compute the propulsion speed near the onset of instability, we use Eq. (S40) to leading order in  $\varepsilon$ :

$$v \approx 2\alpha_c \times \frac{A\varepsilon}{2} \int_0^1 (1 - \cos 2\pi u) du = C\sqrt{\alpha - \alpha_c} \quad (\text{S49})$$

where

$$C = 4\pi^2 \times \sqrt{\frac{1}{\frac{35}{8} + \frac{\pi^2}{3}}} \approx 14.676. \quad (\text{S50})$$

## B. Hairpin shape

We look for rotating solutions of the equations of motion:

$$\mathbf{0} = \mathbf{F}', \quad (\text{S51})$$

$$\gamma^R \boldsymbol{\omega} = \mathbf{M}' + \mathbf{r}' \times \mathbf{F} + \mathbf{m}, \quad (\text{S52})$$

where  $\boldsymbol{\omega}$  is a constant vector. The first equation can readily be integrated to find  $\mathbf{F} = \text{const}$ , and from the stress-free boundary conditions we find  $\mathbf{F} = \mathbf{0}$ . Substituting this into the second equation and differentiating in space, we find

$$\mathbf{0} = \mathbf{M}'' - \delta \mathbf{e}_1''.$$

We expand this equation in the moving frame in terms  $\Pi_2, \Pi_3$  and  $M_1$ , which we take to be a Lagrange multiplier enforcing zero twist  $\Pi_1 = 0$ . We get:

$$(\underline{M}' + \underline{\Pi} \times \underline{M})' + \underline{\Pi} \times (\underline{M}' + \underline{\Pi} \times \underline{M}) = \delta (\underline{\Pi}' \times \underline{e}_1 + \underline{\Pi} \times (\underline{\Pi} \times \underline{e}_1))$$

$$\underline{M}'' + 2\underline{\Pi} \times \underline{M}' + \underline{\Pi}' \times \underline{M} + \underline{\Pi} \times (\underline{\Pi} \times \underline{M}) = \delta (\underline{\Pi}' \times \underline{e}_1 + \underline{\Pi} \times (\underline{\Pi} \times \underline{e}_1))$$

The component-wise equations read:

$$M_1'' + (\Pi_2' \Pi_3 - \Pi_3' \Pi_2) + \delta (\Pi_2^2 + \Pi_3^2) - (\Pi_2^2 + \Pi_3^2) M_1 = 0,$$

$$\Pi_2'' - \delta \Pi_3' + 2\Pi_3 M_1' + \Pi_3' M_1 = 0,$$

$$\Pi_3'' + \delta \Pi_2' - 2\Pi_2 M_1' - \Pi_2' M_1 = 0.$$

These equations are subject to the boundary conditions  $\Pi_2 = \Pi_3 = M_1 = 0$  at both endpoints, giving rise to a nonlinear boundary value problem. The straight configuration  $M_1 = \Pi_2 = \Pi_3 \equiv 0$  is always a solution, but a nonzero one appears at  $\delta = \delta_c \approx 8.99$  as predicted by the linear stability analysis above.

Linearizing the BVP around the straight configuration we find:

$$M_1'' = 0, \quad (\text{S53})$$

$$\Pi_2'' - \delta \Pi_3' = 0, \quad (\text{S54})$$

$$\Pi_3'' + \delta \Pi_2' = 0. \quad (\text{S55})$$

It is easy to see that the linearized system (S53)–(S55) has nonzero solutions only if  $\delta = 2n\pi$  for  $n \in \mathbb{Z}$ , meaning that it has no nonzero solution at the onset of the instability  $\delta = \delta_c \approx 8.99$ . What this implies is that there are no continuously bifurcating solutions of Eqs. (S51)–(S52) from the straight configuration near  $\delta = \delta_c$ , therefore the system must land at the distant fixed point once the straight configuration has become unstable, explaining the finite amplitude jump observed in the angular velocity of the hairpin shapes.

## VI. NUMERICAL METHODS

### A. Integration of shape space equations

The numerical procedure is split into two steps. First, we solve the closed evolution equations for the strain variables  $(\underline{h}, \underline{\Pi})$

$$\dot{\underline{h}} = \underline{v}' + \underline{\Pi} \times \underline{v} + \underline{h} \times \underline{\Omega}, \quad \dot{\underline{\Pi}} = \underline{\Omega}' + \underline{\Pi} \times \underline{\Omega} \quad (\text{S56})$$

where we eliminate the velocity variables  $(\underline{v}, \underline{\Omega})$  via the force and torque balance

$$\gamma^T \underline{v} = \underline{F}' + \underline{\Pi} \times \underline{F} + \underline{f}, \quad \gamma^R \underline{\Omega} = \underline{M}' + \underline{\Pi} \times \underline{M} + \underline{h} \times \underline{F} + \underline{m}, \quad (\text{S57})$$

combined with the constitutive laws for the stresses

$$\underline{F} = \underline{k}^T(\underline{h} - \underline{e}_1), \quad \underline{M} = \underline{k}^R \underline{\Pi} \quad (\text{S58})$$

and the active force and torque densities

$$\underline{f} = -\alpha \underline{\Pi} \times \underline{e}_1 + \epsilon \underline{e}_1 \times (\underline{\Pi} \times \underline{e}_1), \quad \underline{m} = -\delta \underline{\Pi} \times \underline{e}_1 + \beta \underline{e}_1 \times (\underline{\Pi} \times \underline{e}_1). \quad (\text{S59})$$

The closed system of evolution equations for  $(\underline{h}, \underline{\Pi})$  is first order in time and second order in space. The stress free boundary conditions are given as

$$(\underline{h}, \underline{\Pi}) = (\underline{e}_1, 0) \quad \text{at } u = 0, 1 \quad (\text{S60})$$

and we consider an initial condition that corresponds to a small perturbation of the straight undeformed state:

$$\underline{h}(0, u) = \underline{e}_1 + \varepsilon \sin(2\pi u)(0, 1, 1), \quad \underline{\Pi}(0, u) = \varepsilon \sin(2\pi u)(0, 1, 1) \quad (\text{S61})$$

where  $\varepsilon = 10^{-3}$ . The resulting system of six nonlinear PDEs for  $(\underline{h}, \underline{\Pi})$  is solved in Mathematica using the ND-Solve function with the method of lines with adaptive timestepping. We use the following choice of nondimensional parameters throughout our simulations

$$\frac{k_{\parallel}^R}{k_{\perp}^R} = \frac{k_{\parallel}^T L^2}{k_{\perp}^R} = \frac{k_{\perp}^T L^2}{k_{\perp}^R} = \frac{\gamma^T L^2}{\gamma^R} = 10^4. \quad (\text{S62})$$

## B. Reconstruction from shape space trajectory

The second step of the numerical procedure is to reconstruct the rod in space and time, given the velocity and strain variables. We may exploit the  $SE(3) = \mathbb{R}^3 \times SO(3)$  group structure of the rod kinematics [10] in Eq. (1) of the main text by rewriting it as

$$\dot{\varphi} = \varphi \mathcal{V}, \quad \varphi' = \varphi \mathcal{E} \quad (\text{S63})$$

where, in block matrix notation,

$$\varphi = \begin{bmatrix} 1 & 0 & 0 & 0 \\ \mathbf{r} & \mathbf{e}_1 & \mathbf{e}_2 & \mathbf{e}_3 \end{bmatrix} \quad (\text{S64})$$

is an  $SE(3)$ -valued configuration of the rod encoding the centerline and director data, while

$$\mathcal{V} = \begin{bmatrix} 0 & 0 \\ \underline{v} & \hat{\Omega} \end{bmatrix}, \quad \mathcal{E} = \begin{bmatrix} 0 & 0 \\ \underline{h} & \hat{\Pi} \end{bmatrix} \quad (\text{S65})$$

are matrices valued in the Lie algebra  $\mathfrak{se}(3)$  of  $SE(3)$ . We use the notation  $\hat{A}_{ij} = \epsilon_{ikj} A_k$  to associate with each  $\underline{A} \in \mathbb{R}^3$  an antisymmetric  $3 \times 3$  matrix  $\hat{A}$ . Given the velocity field  $V$  and strain field  $E$  and a spatiotemporal discretization of  $[0, T] \times [0, 1]$  we may reconstruct the rod variables in  $\varphi$  by making use of the matrix exponential map and applying a standard Lie-Euler integration scheme [74] to the kinematic equations Eq. (S63). We carry out the reconstruction on a uniform grid  $t_n = n\Delta t$ ,  $u_j = j\Delta u$ . In particular, we carry out a numerical integration of the velocity equation at  $u = 0$  via

$$\varphi(t_{n+1}, 0) = \varphi(t_n, 0) \exp(\mathcal{V}(t_n, 0)\Delta t) \quad (\text{S66})$$

followed by a numerical integration of the strain equation via

$$\varphi(t_n, u_{j+1}) = \varphi(t_n, u_j) \exp(\mathcal{E}(t_n, u_j)\Delta u). \quad (\text{S67})$$

for suitably chosen timestep  $\Delta t = 2 \times 10^{-4}$  and spatial resolution  $\Delta u = 10^{-2}$ .

### C. Computation of the phase diagram

To compute the phase diagram in Fig. 2(g) of the main text, we have solved the shape space equations using the method outlined above up to  $t = 0.5$  for various combinations of  $\alpha, \beta$  with  $\delta = \epsilon = 0$ . Points were then classified as limit cycles if the average time derivative of the curvature of the rod was at least 1 at the end of the integration window. Otherwise, if its average curvature was less than  $10^{-4}$ , it was classified as a straight rod, else as a fixed point.

Linear stability boundaries were obtained by discretizing the linear differential operator on the right-hand side of (S24) using Chebyshev differentiation matrices with 16 nodes and boundary conditions  $\Pi = 0$  and  $\Pi' = 0$  at endpoints. The first two eigenvalues of the linear differential operator were then approximated with the eigenvalues of the corresponding matrix operators.

## VII. LIST OF SUPPLEMENTARY MOVIES

- Movie 1: Fixed point dynamics
- Movie 2: Limit cycle dynamics
- Movie 3: Chaotic dynamics